A EUROPEAN JOURNAL

CHEMPHYSCHEM

OF CHEMICAL PHYSICS AND PHYSICAL CHEMISTRY

Accepted Article

Title: Methane Hydrate in Confined Spaces - An Alternative Energy Storage System

Authors: Lars Borchardt, Mirian Elizabeth Casco, and Joaquin Silvestre-Albero

To be cited as: *ChemPhysChem* 10.1002/cphc.201701250

Link to VoR: http://dx.doi.org/10.1002/cphc.201701250

A Journal of

ChemPubSoc Europe

WILEY-VCH

www.chemphyschem.org

REVIEW WILEY-VCH

Methane Hydrate in Confined Spaces – An Alternative Storage System

Lars Borchardt,[a] Mirian Elizabeth Casco,[a] and Joaquin Silvestre-Albero[b]

Abstract: Methane hydrate inheres the great potential to be a nature-inspired alternative for chemical energy storage, since it allows to store large amounts of methane in a dense solid phase. The embedment of methane hydrate in the confined environment of porous materials can be capitalized for potential applications as its physico-chemical properties such as the formation kinetics or pressure and temperature stability are significantly changed as compared to the bulk system. We review this topic from a materials scientific perspective by considering porous carbons, silica, clays, zeolites, and polymers as host structure for methane hydrate formation. We discuss the contribution of advanced characterization techniques and theoretical simulations towards the elucidation of the methane hydrate formation and dissociation process within the confined space. We outline the scientific challenges this system is currently facing and look on possible future applications for this technology.

1. Introduction

Sir Humphrey Davy is generally credited as the first to provide reliable evidence of chlorine hydrate formation in 1810 [1], though it has been suggested that Priestly observed the phenomenon in 1778.[2] However, it was not until 1930, when this laboratory curiosity became a real industrial nuisance; Hammerschmidt published in 1934 that CH_4 hydrates, instead of ice, were blocking the pipeline in natural gas transmission lines.[3] Three decades later, Makogon discovered natural methane hydrate in Messoyakha gas field in West Siberia Basin and proposed natural gas hydrate deposits as potential energy sources.[4] Since then, significant progress has been made in this field, and occurrence of methane hydrate in nature and prospects for economic recovery has been studied intensively around the world. Natural methane hydrates occur offshore around the globe (in the depth range 300-5000 m) and on land in polar region where the combination of pressure/ temperature/ gas source (microbial and thermogenic) is optimal.[5] The global volume of gas hydrate is enormous; distributed in sediment reservoirs at high saturation (technically recoverable), in massive solid bodies associated with gas venting, and finely-disseminated in shale or filling veins and fractures at low saturation. The energy stored in the estimated 74400 Gt of methane hydrate may be twice that of all other fuels combined.[6] Indeed, the future exploitation of methane hydrate from marine sediments turned out into a priority in the governments' agenda because it may change deeply the global energetic panorama and the relationship between countries. Japan and China have already done a big step extracting methane hydrate, using depressurization technology, from the seafloor in Nankai Trough off in the coast of Japan and in the South China Sea, respectively, and they are planning to establish the commercial production no later than 2030.[7–9] Nowadays, there is a renewed attractive interest in gas hydrate phenomenon in many fields, in particular in material science. Technological methods for water desalinization[10], gas separations[11], carbon dioxide sequestration,[12] and natural gas storage and transportation[13] based on the physico-chemical properties of the gas hydrate are widely investigated. 1 m^3 of solid methane hydrate can release up to 163 m^3 of methane in gas phase at standard condition.[14] As a potential technology to store natural gas, Natural Gas hydrate (NGH), or more elegant Solidified Natural Gas (SNG) is considered to be a cheap and safe alternative to conventional liquefied natural gas (LNG) and compressed natural gas (CNG) because the gas can be stored in solid form under milder conditions. In this regards, Mimachi et al.[15] has reported in 2015, the production of natural gas hydrate pellets that can be successfully stored after 3 months at -20 °C under atmospheric pressure thanks to the self-preservation effect.[16] Despite this big achievement, bulk hydrates are only competitive with LNG for certain niche applications, e.g. where pipeline transport is not feasible and quantities of gas are insufficient for LNG transport.[17]

Additionally, gas hydrate synthesis in the laboratory has still many issues to be addressed. One of the main drawbacks in the gas hydrate formation process concerns the low nucleation kinetics and the high threshold pressure required for the nucleation to start - parameters that would increase the production cost of this technology in an industrial or domestic scale. However, in the last two decades there are already a number of studies that anticipate that these drawbacks can be attenuated in the presence of a solid. By taking advantage of the surface chemistry and the presence of cavities or nanopores, the nucleation kinetics and formation/dissociation threshold pressure can be tailored for a given application. This review highlights the recent developments in the promising field of methane hydrate formation in the confined environment of nanoporous materials, raising the question in the reader´s mind: are methane hydrates in confined space a viable alternative storage system? Intentionally, we discuss this topic from a material point of view, considering designed nanoporous materials, rather than natural sediments. We cover porous materials ranging from silica to porous carbons and polymers. We discuss the challenges that arise in gaining insight into the methane hydrate formation mechanisms by characterization techniques and theoretical simulations. We outline new fields of research and potential applications, this field of research could contribute to and develop in the future.

[a] Dr. L. Borchardt, and Dr. M. E. Casco
Department Inorganic Chemistry, TU Dresden, Bergstrasse 66, D-01062 Dresden, Germany,
E-mail: lars.borchardt@tu-dresden.de
[b] Dr. J. Silvestre-Albero
Laboratorio de Materiales Avanzados, IUMA, Universidad de Alicante, Ctra. San Vicente del Raspeig-Alicante s/n, E-03690 San Vicente del Raspeig, Spain.

Dr. Lars Borchardt obtained his PhD in Inorganic Chemistry in 2013 at the TU Dresden (Germany). After postdoctoral stay at the ETH Zürich, he became leader of a junior research group at the TU Dresden. His research focuses on chemical energy storage systems based on methane hydrate as well as electrochemical energy storage in supercapacitors and Li-S batteries.

Dr. Mirian Elizabeth Casco obtained her PhD in Materials Science at the University of Alicante (Spain) in 2015. She is currently working at TU Dresden (Germany) as a postdoctoral fellow supported by Alexander von Humboldt foundation. Her research experience covers the synthesis and characterization of porous materials for gas adsorption/separation and natural gas storage applications.

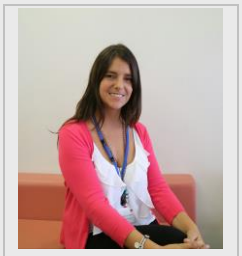

Dr. Joaquin Silvestre-Albero obtained his PhD in Inorganic Chemistry at the University of Alicante in 2003. After a post-doctoral stay at the ITQ Institute in Valencia (Spain) and at the FHI Institute in Berlin (Germany), he became Assistant Professor (2006-2011), and Associate Professor (2011-till date) at the University of Alicante. His main expertise is the design and characterization of porous solids for gas adsorption/storage and biomedical applications.

2. Properties of Methane Hydrate

Gas hydrates - also called clathrate hydrates - are crystalline solids that form when water and certain gases such as SO_2, CH_4, CO_2, ethane, or H_2 come into contact under thermodynamically favorable conditions that is, when the temperature and pressure conditions pass through the equilibrium T-P curve for gas hydrate formation. For instance, at 2ºC for bulk methane hydrate this is around 3.18 MPa.[18] Gas hydrates are inclusion compounds that comprise H-bonded water molecules (host) that provide cages which can allocate gas molecules (guest). The structure is maintained stable due to the van der Waals forces between the host and the guest.

Gas hydrate is also described as a solid solution, in which one or more solutes (guest) are immersed in a solvent (host framework). Based on this assumption, in 1959 van der Waals and Platteeuw developed the statistical thermodynamic model to described the chemical potential of water in the hydrate phase and provides the tools to predict the equilibrium conditions in free water.[19] There were several updates to this model, nicely summarized and reported by Sloan.[2] The main conclusion that has been drawn is related to the stability of the gas hydrate that directly depends on the water activity. The capillary effect induced by geometric constrains in confined space, the chemical nature of the pore walls or/and the presence of inhibitors (salts and alcohol) are some of the factors that exert strong influence in the water activity and change the thermodynamic properties and phase equilibrium of confined gas hydrates. The following equation shows the decrease of water activity as a function of the shape, size and surface characteristic of pore[20,21]

$$lna_w = ln(x_w\gamma_w) - {FV_L cos\theta\sigma_{HW}}/{rRT} \quad \text{Eq. 1}$$

where F is the shape factor reflecting curvature of the hydrate-liquid interface, V_L is the molar volume of pure water, θ is the wetting angle between pure water and hydrate phases, σ_{HW} the interfacial tension between hydrate and liquid water phases, r is the pore radius, $x_w\gamma_w$ is the product of water concentration and the activity coefficient. We direct the reader to the review of Kim and Lee who nicely described the phase behavior of gas hydrates in nanoporous materials.[22]

2.1. Crystal structure

The three main crystal structures are named structure I (sI), structure II (sII) and hexagonal (sH) **(Figure 1)**.

Structure I is the most common for methane hydrate in nature. It contains two small cavities (radius 0.391 nm) formed by twelve pentagonal faces, denoted by $2(5^{12})$, and six large cavities (radius 0.433 nm) containing 12 pentagonal and 2 hexagonal faces, denoted by $6(5^{12}6^2)$. The average cavity radius varies with temperature, pressure and guest composition. Small molecules apart from methane stabilize this structure, such as CO_2 and ethane. The cubic unit cell has a size of ca. 1.21 nm. The ideal composition for methane hydrate would be $8\ CH_4 \cdot 46\ H_2O$ (or $CH_4 \cdot 5.75\ H_2O$).[2] *Structure II* is formed by 16 small cavities (radius 0.391 nm) containing 12 pentagonal faces, 16 (5^{12}), and eight large cavities (radius 0.473 nm) with 12 pentagonal and four hexagonal faces, $8(5^{12}6^4)$. Big molecules up to 6.6 Á, such as propane and iso-butane can stabilize the large cavities, while the small cavities remain empty. The cubic unit cell has a size of ca. 1.72 nm and contains 24 cavities and 136 H_2O molecules.[2] Finally, the *Hexagonal Structure* is formed by three small cavities (radius 0.394 nm) containing 12 pentagonal faces, $3(5^{12})$, one large cavities (radius 0.579 nm) with 12 pentagonal and eight hexagonal faces, $(5^{12}6^8)$, and two medium cavities (radius 0.404 nm) containing three square, six pentagonal and three hexagonal faces, $2(4^35^66^3)$. Two guest molecules are needed to stabilize sH crystals, e.g. CH_4 or H_2S in the small or medium cavities with big molecules such as 2,2-dimetylbutane in the big cavity. The ideal composition of the hexagonal unit cell is 6 (cavities) $\cdot\ 34H_2O$ with edges of ca. 1.22 nm and ca. 1.01 nm.[2]

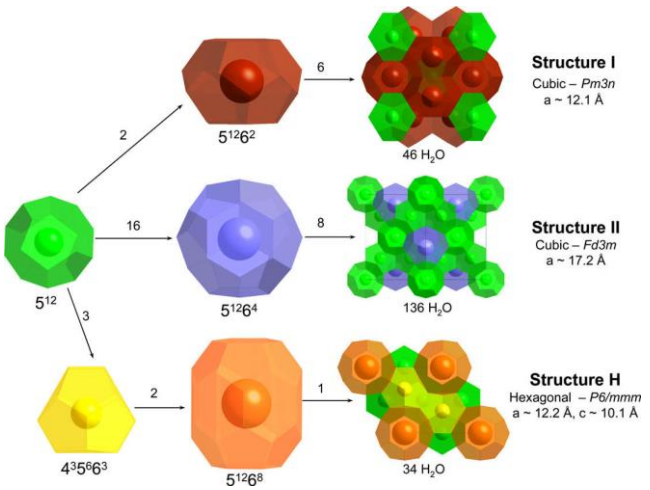

Figure 1. Common clathrate hydrate structures. Reprinted with permission from [23]. Copyright (2017), with permission from Elsevier.

2.2. Hydrate formation

Methane hydrate (MHs) formation is a two-main-step mechanism of the nucleation and the growth around the formed nucleus.[24] The critical step is the nuclei formation since water molecules have to create the critical size cluster in cooperation with gas molecules.[25] The nucleation occurs during the induction time, and highly depends on the condition settings (e.g. pressure, temperature), but it is particularly slow in bulk water when the liquid-gas interface is restricted. Afterwards, the nuclei grow and a thin film of MHs is created at the interface and further crystal growth is limited by the diffusion of the gas through it. As a result, artificially synthesized gas hydrates not only takes many days, but also is typical to have a low water to hydrate conversion (i.e. unreacted interstitial water), thus making the process very inefficient for practical application.

Common strategies to overcome both issues consist of subcooling systems with vigorous stirring, in which the gas is injected into bulk water or vice versa.[26] Zhong and Rogers[27] have shown that anionic surfactants and biosurfactants can greatly enhance the rate of nucleation and growth of natural gas hydrates in quiescent systems, reducing the formation time from few weeks to few hours.[28] Mori et al.[29], supported by several works[30–32] have stated that the major mechanism of the hydrate-formation enhancement is the capillary-driven supply of water into porous hydrates layer growing on the walls of the hydrate-forming chambers and not the formation of micelles which, in any case, would retard the hydrate formation[33]. In contrast to the various emulsion and suspension techniques,[34] and the different surfactants[35,36] that have successfully been used to increase nucleation kinetic, inhibitors have also been widely investigated to prevent the crystals from agglomeration and subsequently pipeline blockage[37]. Current practices are to avoid hydrate blockages by injecting an alcohol- or glycol-based thermodynamic hydrate inhibitor (THI).[38] THI shifts the equilibrium hydrate dissociation/stability curves to a lower temperature and higher pressure based on colligative properties, and decreasing the water activity.[39] However, under a high degree of supercooling, large amount of THI becomes non-viable. Addition of low dosage of kinetic hydrate inhibitors (e.g. polymer-based inhibitor[40] or more recently, ionic liquids and amino acids have been proposed[41,42]) can slow down the hydrate nucleation rate long enough to overpass the residence time of methane and water mixture in the transport pipelines.[43]

Many authors have investigated the role of porous media in gas hydrate nucleation and growth. Porous silica is often selected to emulate different geological sediments, whereas other porous materials such as activated carbon and metal-organic frameworks have been investigated as platforms to store gas in form of hydrate. Because of their tuneable porosity, modulated chemical surface together with the confinement effects, porous materials are excellent candidates to promote the nucleation and growth in static conditions and maximise the water to hydrate conversion. All these aspects dealing with confinement effects in porous media (from carbon materials and silica to clays and polymers) will be covered in the next sections.

3. Confined Spaces

Since this review addresses particularly nanoporous materials as host structures for the growth of methane hydrate, the authors considered it pivotal to outline the major feature of porous structures, which is the “confinement effect”.

A cavity (pore) inside a solid that has a lateral dimension of only a few molecular diameters can change the physico-chemical properties of incorporated guest molecules (fluid phase) tremendously. The reduced number of neighbor molecules and the antagonism between fluid-fluid and fluid-pore interactions involve the so-called confinement effect. This effect entails the shift and the appearance of new phase transitions as compared to the bulk system.[44] The van der Waals interaction between a molecule and a surface strongly depends on the curvature of the latter.[45,46] On a theoretical basis, Derouane described this relation by **equation 2**, with the van der Waals energy *(W)* and radius *(d)* of a molecule, which is confined in a micropore with the radius *(a)*. The parameter *s (s=d/a)* describes the ratio between the molecule and pore size and can vary between 0 and 1. Thereby, s=0 represents a flat surface and s=1 the entire fitting. It follows that for the latter case the van der Waals Energy is 8-times larger than for the corresponding flat surface.

$$W = \frac{-C}{4d^3\left(1-\frac{s}{2}\right)^3} \qquad \text{Eq. 2}$$

This explains the deviating behavior of confined molecules as compared to their bulk phases such as supermobility, strong physisorption, high heats of adsorption, varying catalytic properties and many others.[45] The confinement effect can also be described from a quantum theoretical perspective. Typically, the molecular orbitals of a material span over its unlimited region of flat surface. However, if this surface is confined the limited boundaries involve the increase of the orbital energies. This will influence the electronic structure of any guest molecules entering this space and result in a deviating interaction.[47] With this, first order phase transitions like melting and freezing are

impacted. Many investigations were conducted on porous silica materials with ordered and thus uniform pore sizes. All these experiments have shown that the freezing point inside the pore is depressed with respect to the corresponding bulk phases and this effect becomes even greater with smaller pores.[48] For instance, liquid water can be thermodynamically stable in silica micro- and small mesopores at temperatures below the limit of homogeneous bulk nucleation (~235 K).[49] Das et al. have calculated the melting transition in slit and cylindrical pores.[50,51] They reported that for narrow hydrophobic pores there is oscillatory behavior of the melting transition depending on the pore radius.

The thermodynamic conditions inside confined environments can be dramatically different from the bulk environment. For instance, high pressure phases and high pressure chemical reactions are observable in confined spaces at pressures, which are orders of magnitudes lower than commonly required for the bulk system. Gubbins and co-workers calculated that the tangential in-pore pressure (i.e. the pressure parallel to the wall) can reach tens of thousands of bars, even though the bulk pressure outside the pore remains at ambient conditions. This in-pore pressure is very sensitive to small changes of the bulk pressure and the pore size.[52] It is crucial to consider, that a confined space is a highly complex system and a way more contributions need to be taken into account, such as metastable states of the fluids, surface heterogeneities and pore connectivity effects.[48] In the context of this review, we will discuss materials of different pore size. We distinguish between macropores (pore diameter, d_p > 50 nm) potentially hosting hundreds and thousands of units cells, mesopores (2 < d_p < 50 nm) that can host a few up to tens of unit cells, and micropores (0 < d_p < 2 nm) that can host max. 1 unit cell (approx. 1.2 nm) of MH. The readers should be aware that there is no characterization so far that shows the methane speciation in pores, especially in micropores. Indeed, owing to the steric hindrance, micropores even do not allow the growth of a regular methane hydrate crystal.

4. Methane Hydrate in Confined Spaces

As described above, one of the main drawbacks in the nucleation and growth of gas hydrates in bulk water concerns the slow kinetics. This is due to the limited gas-liquid interphase (interfacial phenomena) that inhibits appropriate methane dissolution/diffusion (mass transfer resistance) in bulk water to reach the critical concentration required to initiate the nucleation. Furthermore, the bulk process is also limited by the agglomeration of hydrate crystals at the interface, so that the formation rate is inversely proportional to the thickness of the hydrate film.[35,36] However, these limitations can be overcome through the incorporation of a solid surface able to improve/promote the contact area between water and methane, thus speeding-up the nucleation kinetics. In the specific case of solids containing cavities or holes, there is a second effect due to the presence of confinement effects, i.e. due to the presence of a large adsorption potential in narrow cavities. Celzard et al. nicely described how these capillary effects in pores could alter the gas hydrate formation pressure compared to bulk water (i.e. P_{fw} = 3.18 MPa at 2ºC).[18] According to **equation 3**, for a cylindrical pore having a width w the capillary pressure ΔP varies according to:

$$\Delta P = \frac{4\sigma_{lh}\cos\theta}{w} \quad \text{Eq. 3}$$

where σ_{lh} is the surface tension between liquid water and hydrate phases, onto which water spreads with a contact angle θ, that is assumed to be zero. The hydrate formation pressure (P_f) compared to bulk water (P_{fw}) is then

$$P_f = P_{fw} + \Delta P \quad \text{Eq. 4}$$

Based on **equation 4**, at low pressures methane hydrate formation must take place in the widest pores, while a further increase in pressure promotes hydrate formation in smaller pores. For instance at 3.5 MPa and 2ºC those pores with mean diameter above 300-350 nm participate in the hydrate formation process, while hydrate formation in mesopores (2 < w < 50 nm) require pressures above 5.3 MPa, assuming that water is still liquid in such pores.[18] As described above, the sI structure of the clathrate hydrate of methane is centred cubic with a lattice parameter of ca. 1.2 nm.[2] Taking into account that hydrate formation in pores requires the presence of an interfacial liquid film between the hydrate crystal and the solid pore walls,[55] the estimated pore width for the gas hydrate to crystallize must be close to the border between micropores and mesopores, i.e. around 2 nm. Based on this assumption, one would expect a minor contribution of the microporosity for trapping methane by hydrate formation, at least in a perfectly crystalline network. Last but not least, the methane hydrate formation process (threshold pressure, storage capacity, water-to-hydrate yield, etc.) highly depends not only on the porous structure but also on the nature of the solid material selected, as will be discussed in the next sections.

4.1. Methane hydrate formation in carbon materials

Porous carbon materials have attracted considerable attention in recent years in a wide variety of applications, including methane storage.[56,57] One of the main advantages of carbon materials is that the synthesis method can be tailored to achieve carbon materials with a perfectly designed porous structure (from purely microporous carbons to hierarchical structures combining different pore sizes).[58] In the same way, surface chemistry can be designed by a proper choice of the carbon precursor or through the application of post-synthesis methods (e.g. thermal treatment under a specific gas atmosphere). The large versatility in the synthesis procedure and the large variety of carbon sources makes carbon materials a highly promising candidate to host gas hydrates under confined environment.

One of the pioneering studies in methane hydrate formation using carbon materials as a host structure dates back to 1998. Miyawaki et al. evaluated the methane adsorption in purely

microporous carbon materials and activated carbon fibers.[59] These results proved that the presence of pre-adsorbed water gives rise to a remarkable enhancement of methane adsorption, even for microporous samples. The enhanced methane adsorption strongly depended on the amount of the pre-adsorbed water in micropores. Due to the restricted space in micropores, these studies suggested a composition for the stable molecular compound methane/water = 1:2, far from the stoichiometric value ($1CH_4 \cdot 5.75H_2O$). Contrary to steric assumptions described above, micropores promote the formation of a two-dimensional stacked structure called methane nanohydrate. This structure constitutes a monolayer of methane molecules adsorbed in the graphitic pore walls, while water molecules repelled from the walls are associated with each other to form a hydrogen-bonded zigzag chain at central space of the micropores. Minimum pore width for abundant formation of methane nanohydrate was set at 1.05 nm.

A similar enhancement in the methane adsorption capacity under wet conditions was described for microporous and micro/mesoporous materials by Celzard et al. and Zhou et al. [18,60,61] At pressures below 4 MPa the methane adsorption isotherms correspond to a classical adsorption hindered by the presence of water (micropore filling and micropore inaccessibility take place), while a crossover phenomenon associated with a step takes place in the isotherm above 4 MPa. Interestingly, this crossover reaches a plateau for microporous carbons with a low activation degree due to the saturation of the porosity with hydrate. On the contrary, on samples with a highly developed porosity (containing large micropores and mesopores) methane hydrate formation continues up to high pressures (above 6-7 MPa), most probably associated to the larger accessibility of methane to the inner water-filled micropores in the last samples. These three processes, i.e. pore inaccessibility, methane hydrate formation in large pores and methane hydrate formation in small meso- and micropores, can be clearly appreciated in **Figure 2** for a petroleum-pitch derived activated carbon with a highly developed porous structure.[62] As described before, below 3 MPa the amount of methane adsorbed is rather zero due to the blocking effect exerted by water. Above this pressure, the methane isotherm exhibits a sudden jump that coincides with the pressure of bulk hydrate formation (3.8 MPa at 2ºC).

According to **equations 3 and 4**, this step must be unambiguously associated with methane hydrate formation in large pores or cavities being rather reversible. As the pressure increases, there is a second enhancement above 6 MPa and up to 10 MPa, associated with a large hysteresis loop, and attributed to the methane hydrate formation in the inner cavities of the activated carbon (mesopores and wide micropores). In these small cavities a larger pressure is required not only due to the capillary effects on small cavities, as described above, but also due to the slower methane diffusion through a porous network partially and increasingly occupied by clathrates. The beneficial effect of larger pores promoting methane diffusion through the hydrate network has been clearly addressed by Borchardt et al. using porous model carbon materials.[63] Compared to the dry samples, the presence of pre-adsorbed water, up to saturation, gives rise to an improvement in the methane adsorption capacity from 18.4% for a purely microporous carbon (pore size 0.8 nm), up to 120% and 170% improvement for mesoporous carbon materials with 10 nm and 25 nm mean pore size, respectively. The larger water-to-hydrate yield in mesoporous materials clearly supports the necessity of appropriate methane diffusion for an optimum conversion. Water-to-hydrate yields above 95% have also been addressed in the literature for activated carbons with a highly developed mesoporosity.[64,65]

Siangsai et al. also investigated the role of the carbon particle size in the water-to-hydrate yield.[64] Experimental results show that the highest average water to hydrate conversion (96.5%) takes place with the largest particle size (841-1680 μm), due to its large interstitial pore space between the activated carbon particles, whereas the highest methane recovery (98.1 %) was achieved with the smallest fraction (250-420 μm). The water conversion to hydrate (%) was calculated using the hydration number of 6.1. Furthermore, the temperature profile during the methane hydrate formation shows the exothermicity of the process with two well-defined temperature spikes, the first one due to gas hydrate formation in the first water-film followed by a secondary growth process in the cracks formed within the previously formed film.[64] Not only the porous structure has an effect in the methane hydrate formation, but also the surface chemistry of the carbon material. As recently described by Casco et al. the incorporation of oxygen-containing surface groups modifies the water activity and water distribution within the carbon sample, thus promoting the methane hydrate formation at lower pressures (around 3-4 MPa).[66] Apparently, the preferential location of oxygen groups at the pore mouth promotes water clustering in larger pores (micropores are not filled with water), thus promoting the hydrate formation at lower pressures, in close agreement with the pore size effect discussed above.

Coming back to the kinetics, the slower diffusion of methane in the high-pressure region has been widely addressed in the literature.[18,61,62] Whereas a few tens of minutes is usually sufficient for each adsorption point in the methane isotherm to reach equilibrium in the case of dry adsorbents, several hours or days are required for the wet carbons, mainly for pressures above P_f. These large time-scale values are due to the presence of several step in the methane hydrate formation mechanism, i.e. i) methane dissolution into water until a critical concentration is achieved, ii) stochastic nucleation of small hydrate nuclei and their dissociation until a critical cluster radius is formed (induction period), and iii) growth step until a phase equilibrium is achieved at both the water/hydrate interphase and the gas/water interface. Govindaraj et al. compared the formation kinetics in the presence of a suspension of activated carbon and nano-silica.[67] Although both systems have promoting effects on methane hydrate formation kinetics, the effect of activated carbon was significantly more pronounced (induction time in the presence of activated carbon is around 30 min, while for nano-silica is around 84 min). However, the final storage capacity under water-excess conditions (nanoporous suspensions) is rather low (around 12-20 V/V) compared to similar experiments

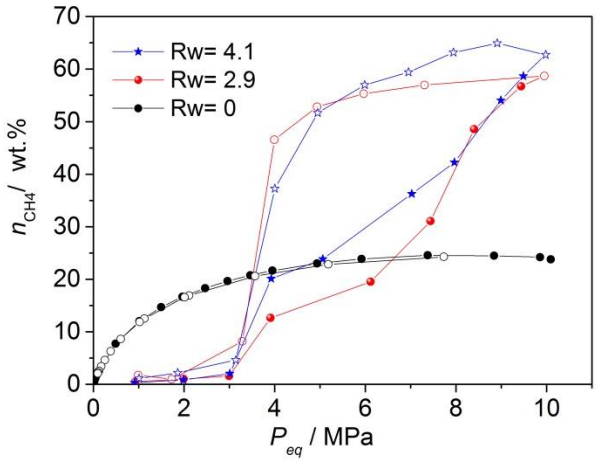

Figure 2. High-pressure methane adsorption isotherm at 2 ºC for a petroleum-pitch derived activated carbon pre-saturated with water (2.9 g/g and 4.1 g/g). The isotherm of the dry carbon is included for the sake of comparison. [62]

in fix bed reactors using wet-carbons (around 210-250 V/V).[61,65,68]

Nucleation kinetic can also be enhanced through the incorporation of promoters. For instance, cationic or anionic surfactants such as sodium dodecyl sulphate or cetyl tri-methyl ammonium bromide (CTAB),[18,27,69] or even nano-copper suspensions for HFC134a gas hydrates,[70] have been widely investigated in the literature either confined in porous materials or in bulk conditions to decrease the surface tension of water and to increase the diffusion rate of gas into water. The effect of the promoter depends on its nature and the final conditions applied. However, the topic of the promoters is outside the scope of this review and it will not be covered here.

Concerning the methane hydrate formation mechanism, there is some controversy in the literature in the understanding of the formation process in confined nanospace.[68,71]

The existence of methane hydrate in marine sediment confirms the observation that hydrate can nucleate in a saturated methane solution – without the presence of a gas/water interface.[72] In the confined nanospace, water forms a water film inside the carbon cavities, thus improving the contact area between methane and water. Under these circumstances, the formation process will imply three steps: i) liquid water films formed on the surface of the carbon particles, ii) initiation of the hydrate formation at the water/carbon interface, the further growth of hydrate is controlled by the transfer rate of methane through the water film and iii) the phase equilibria are achieved at both the water/hydrate and gas/water interface (see **Figure 3**).[68] Under these conditions the total hydrate formation rate in wet carbon is defined by **equation 5**:

$$-\frac{dn}{dt} = K_L \cdot A_L (x_i - x_e) \qquad \text{Eq. 5}$$

Where K_L and A_L are the coefficient of mass transfer of gas through liquid film and the total area of mass transfer between gas and water, respectively. x_i and x_e constitute the concentration of methane in the water film near the water/vapor interface and that near the water/hydrate interface, respectively. Thus, $x_i - x_e$ constitutes the driving force of the mass transfer of methane through the water film between the gas phase and the hydrate.[68]

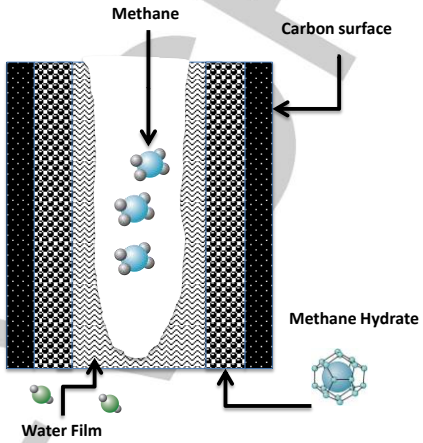

Figure 3. Schematic representation of the methane hydrate formation process in carbon pore.

This formation mechanism was confirmed by Babu et al. using a microscope coupled to a high pressure crystallizer.[73] These *in-situ* observations showed that hydrate formation starts on the surface of the activated carbon, although the formed metastable nucleus dissociate after some period of time (*ca.* 150s), within the hydrate formation region (pressure and temperature in the hydrate stability region). This phenomenon is known as the transient hydrate crystal formation/dissociation within the hydrate stability region. Jung and Santamaria reported similar observations for the methane hydrate formation in capillary pores.[74] Apparently the thin layer of water wetting the activated carbon particle is not able to sustain the hydrate growth after nucleation, resulting in a transient hydrate formation/dissociation. However, this phenomenon disappears for small carbon grains. The authors attributed this observation to the beneficial effect of interconnectivity of the pore space to facilitate the crystal nuclei to further grow and sustain hydrate growth thereafter.

Taking into account the above-described mechanism, the formation of a water film on the carbon surface is the key factor to speed-up the hydrate formation process compared to the bulk phase (lowering the mass transfer of gas through the liquid). Consequently, the amount of water incorporated (R_w) must play a crucial role defining not only the formation kinetics, but also the water-to-hydrate yield. As widely described in the literature, the amount of methane stored as a hydrate increases with R_w up to a maximum or optimum wetting, depending on the carbon material and the experimental conditions. Larger water loadings limit the diffusion pathways through the pore network, the amount of gas hydrate formed decreasing drastically.[18,59,68]

Last but not least, one of the main difficulties under confinement conditions concerns the identification and evaluation of the hydrate crystals formed. Among others, inelastic neutron

scattering (INS) and synchrotron X-ray powder diffraction (SXRPD) have been proved to be valuable techniques to learn about the spectroscopic behavior (vibrational and rotational modes) and crystal structure of these confined systems.[62,63] As recently pointed out by Casco et al.[62] the confined hydrates preserve the spectroscopic fingerprint of natural hydrates from the Pacific Ocean, with the free rotor of CH_4 encapsulated in ice-like cages clearly visible in the low energy transfer region. Furthermore, crystallographic observations unambiguously show the presence of sI structure for the confined hydrates, with a stoichiometry of *ca.* $1CH_4{\cdot}5.8H_2O$, preferentially for hydrate formation in large pores or cavities.[62] Smaller pores exhibit a certain water deficiency maybe due to the presence of non-stoichiometric hydrates, due to steric constrictions, or to the presence of some non-associated physisorbed methane.[61,62]

The promoting effect of carbon materials for methane hydrate formation has not been restricted only to activated carbon or activated carbon fibers. There are also some examples in the literature of promoting effects after incorporation of carbon nanotube suspensions. For instance, Park et al. observed that the incorporation of 0.004 wt.% of multi-walled carbon nanotubes (MWCNTs) to pure water could enhance the amount of methane consumed more than 300%. Furthermore, the presence of MWCNTs gives rise to a decrease in the hydrate formation time at a low subcooling temperature[75]. A similar performance was observed for functionalized multi-walled carbon nanotubes with an optimum in the gas consumption at 0.003 wt.% MWCNT attributed to the rapid hydrate layer formation at the boundary of the gas and nanofluid.[76]

The presence of confinement effects in carbon cavities have a promoting effect in the nucleation kinetics compared to bulk phase. Interestingly, the promoting effect of carbon materials is also reflected in the thermodynamics of the hydrate formation process. As described by Handa et al., the presence of geometrical constraints in the pore cavities has an effect in the activity of water (similar to natural sediments where water activity is altered due to the presence of dissolved salts and capillary forces in the compacted sediments), that is reflected in the phase-equilibria and thermodynamic properties of the hydrates formed.[77] When confined in small pores and/or in the presence of interacting surfaces, the thermodynamic properties of hydrates change the same way as those of ice. The dissociation pressure of the confined hydrates is higher than that of the bulk hydrates, i.e., pore hydrate is less stable than bulk hydrate. For instance, Borchardt et al. described a small destabilization of the confined hydrates irrespective of the adsorption temperature and the mean pore size of the model carbon materials evaluated. [63]

All measurements described in the literature for methane hydrate formation in confined nanospace using carbon materials as a host structure are dealing with pure water. However, the information obtained under these “ideal conditions” cannot be extrapolated to other liquid media (for instance, seawater environments). This is important not only to understand the performance of natural hydrates, where salty water is the liquid media, but also in the case of synthetic gas hydrates. This is the case, for instance, in a future scenario based on artificial gas hydrates platforms as a safe reservoir to be located in the coastline for high energy-demanding countries. Recent studies from Cuadrado-Collados et al. have shown that salty water has an important effect in the water-to-hydrate yield due to entropic effects (salty water inhibits the methane hydrate formation).[78] However, these drawbacks can be minimized working at temperatures below the water freezing point (e.g., -10ºC), with a good performance compared to pure water in terms of total adsorption capacity (66 wt.% CH_4 vs. 93 wt.% for seawater and pure water, respectively, at -10ºC and 10 MPa), water-to-hydrate yield and nucleation kinetics. These values constitute an improvement of 128 and 220 % compared to the dry sample in terms of methane adsorption capacity, thus opening the gate for a future application of this methane hydrate technology in seawater environments using activated carbon as a host structure.

4.2. Methane hydrate formation in silica and silica sand

The evaluation of the methane hydrate formation process in silica and silica sand has been widely addressed in the literature. This research has been motivated by the necessity to understand the natural process, where gas hydrates grow in pores of coarse-grained sediments (e.g., in carbonates and silicates) or fractures in geostrata. As nicely described by Handa and Stupin, the stability conditions of clathrates hydrates depends directly on the activity of the confined water.[77] As described above, the water activity decreases in the confined space of porous materials, with the associated increase in the threshold pressure for methane hydrate formation at a given temperature or a decrease in the temperature at a given pressure. From this perspective, in the natural media the water activity will be affected by the capillary forces in the compacted sediments and by the presence of dissolved salts[79]

A systematic study by Uchida et al. using porous glasses with different pore sizes (from 10 to 50 nm) suggested that the temperature offset for hydrate dissociation is in inverse proportion to the pore diameter, i.e. dissociation temperature decreases with the silica glass pore size.[80] By applying the Gibbs-Thomson effect, they provided a mathematical explanation of the relation between pore size and phase equilibrium data, at constant pressure (the Kelvin equation has to be applied at constant temperature):

$$\frac{\Delta T}{T_d} = 4\,\gamma_{HW}(\rho_H L_H d)^{-1} \qquad \text{Eq. 6}$$

where γ_{HW} is the hydrate-water interfacial free energy, $\rho_H$is the density of methane hydrate, L_H is the latent heat of the dissociation of pores hydrates, d is the pore diameter, and $\Delta T = T_d - T_e$, T_d and T_e are the dissociation temperatures of methane hydrate in confined pores and in bulk phase, respectively.

This observation is in close agreement with **equations 3 and 4** described above. The Arrhenius plot suggest that the methane-hydrate dissociation heat tends to be small in pores below 30 nm compared to the bulk phase. The density of the methane

hydrate was estimated to be 914 kg/m^3, with an apparent interfacial free energy between hydrates and water in the confined conditions to be around 3.9 x 10^{-2} J/m^2, which is comparable to that between ice and water.[79] A similar conclusion concerning the dissociation pressure in pore hydrates (thermodynamically the pore hydrates are less stable than the bulk hydrates, maybe due to the finely dispersed state in confined space) was reported by Handa et al. for 7 nm radius silica gel and Uchida et al. for Vycor porous silica glasses from 4 to 100 nm.[77,81] Handa et al. reported the heat of dissociation for hydrates in pores to be around 45.92 kJ/mol, which is smaller than that of the bulk (54.19 kJ/mol). Indeed, the enthalpy of hydrate formation in porous media decreases as the pore size decreases. Anderson et al. described a conceptual model to understand the hydrate equilibria and hydrate inhibition in mesoporous silica.[55] Interestingly, using calorimetric data upon heating, Handa et al. observed that after the initial hydrate dissociation into ice and gas, the hydrate became totally encapsulated by the pore walls and the ice caps formed at the pore opening. The hydrates trapped in the interior of the pore remained stable up to the melting point of ice. These results were in close agreement with bulk hydrate studies where shielding stabilization effects by ice layers could be observed.[82] Hu et al. observed a similar self-preservation effect for methane hydrates formed in dry-water (although more than half of the total methane could be released before the self-preservation occur).[83] More recently, Mel´nikov et al. have observed the anomalously low rates of dissociation of gas hydrate in dry-water dispersion with a stabilizer content of 5 wt.% (hydrophobized silica particles) at a temperature below 273K and a pressure of 0.1 MPa.[84] The self-preservation effect was also observed by Hachikubo et al. in glass beads. [85]

Methane hydrate formation in large-scale reactors was studied by Linga et al. Using different volume bed of silica sand particles (average diameter equal to 329 μm), the authors observed nucleation events occurring at different times (rates) and different locations within the bed (preferentially for the experiments at 4ºC).[86] Furthermore as the bed size become smaller, the degree of temperature increase due to the multiple nucleation and hydrate formation becomes smaller. Most probably, as the silica sand bed becomes thinner, the contact with the external copper cylinders is more effective, and the heat released is removed faster from the crystallizer. The formation of methane hydrates was confirmed by Raman spectroscopy and morphological observations. Compared to a stirred vessel, fixed bed experiments in the presence of silica sand gave rise to a more extensive formation of hydrate crystals with conversion values close to 94.7% in 34h (vs. 74% after 60h in the stirred vessel).[53] Although the majority of these studies are performed using pure water, Nair et al. evaluated the performance of several silica sand samples with different particle size in the presence of seawater from coastal Chennai (India).[87] The gas consumption and indirectly the hydrate formation was larger in the presence of smaller size sand particles in both pure and seawater. However, the total consumption was less in the presence of seawater as compared to pure water. Also the gas recovery and dissociation rates were found to be higher in the smaller size silica sand bed in pure water as compared to the bigger ones and seawater. These authors proposed a two steps formation mechanism. A first step taking place 1-2h after gas injection attributed to the formation of a hydrate film in the meniscus formed in the pore space between sand particles, and a second step after 6h due to further hydrate growing in the cracks formed in the initial hydrate layer (see **Figure 4**). These cracks can be formed due to the pressure difference between the two sides of the hydrate layer (high-pressure gas phase in one side and enclosed water phase in the other side). This two-step growth mechanism was proposed previously by Jin et al. [88] in water- unconsolidated sand particles using attenuated total reflection infrared (ATR-IR) spectroscopy and optical microscopy observation.

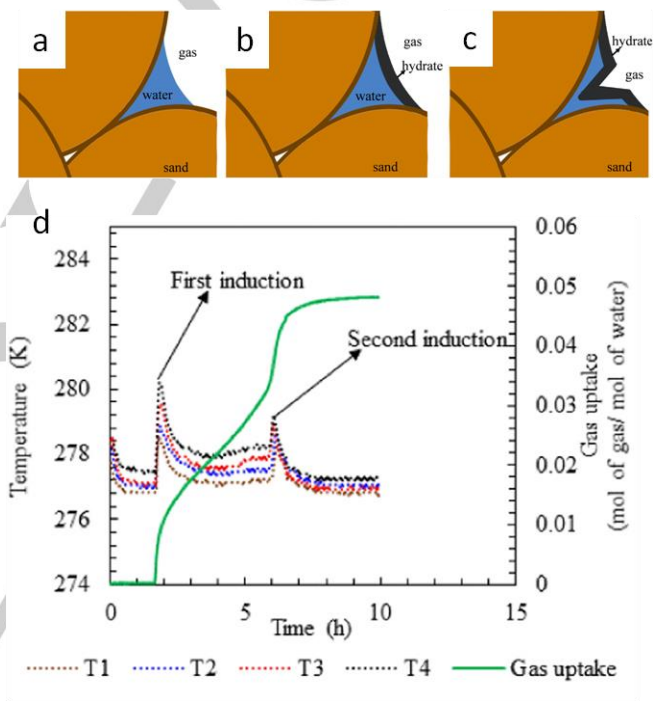

Figure 4. Representative scheme a) before hydrate formation, b) first stage hydrate growth, and c) second stage hydrate growth in the pore space between sand particles, and d) temperature profile and gas uptake curve for 0.16 mm sand sample (T1, T2, T3, T4 are temperature sensors fixed at various locations in the experimental set up). Reprinted with permission from [87]. Copyright (2017), with permission from Elsevier.

Wang et al. reported the formation of methane hydrate in dry water (DW) with an excellent performance in terms of storage capacity (storage capacity above 175 v/v at 273.2 K) compared to the bulk system in the absence of silica (storage capacity close to 0).[34] This promoting effect was attributed to the large surface area/volume ratio compared to the bulk phase. Furthermore, these experiments suggested that the methane storage capacity depends on the average water particle size. Although the induction time is rather similar for all particles (typically 5-10 min), larger particles exhibit a lower water-to-

hydrate yield. Unfortunately, these studies using DW does not take advantage of the confinement effects (silica H18 particles are non-porous), with the associated drawbacks related with water-droplet agglomeration after different freeze-warm cycles, and the subsequent degradation in the storage capacity and formation kinetics. These drawbacks can be avoided by using hollow silica as a host structure. Using water-saturated silica spheres, Prasad et al. demonstrated that hollow silica promotes the methane hydrate formation to a similar extend (hydrate conversion efficiency ≈ 40%) either under stirred or nonstirred conditions, i.e. stirring could be eliminated.[89] However, the formation kinetics in silica slurry under nonstirred conditions was slower. High and fast hydrate conversion could be optimized by adjusting the water to silica ratio with more than 90% conversion and a storage capacity above 206 v/v.[90]

4.3. Methane hydrate formation in clays and zeolites

Clay minerals have also been widely evaluated as a host structure for methane hydrate formation since clay minerals are also representative of geochemical components comprising sediments. Most geological clays are phyllosilicate minerals constituted by a stacking arrangement of layers in perpendicular direction, and various metal cations and water molecules allocated in the interlayer space. These morphological characteristics and the associated swelling of the interlamellar space for some clays, depending of the amount of water, makes the hydrate formation in clays a complex process compared to other more rigid systems like carbon materials or silica. Kim et al. proposed three steps for the water swelling on montmorillonite depending on the loading: i) crystalline swelling where the interlayer spacing increases from 0.95 (dry state) to around 2.0 nm (for water loading between 27 and 54 wt.%) at 99% relative humidity, ii) water swelling upon contact with water with a 20-fold expansion of the clay volume with interlayer spacing above 2.0 nm and iii) the formation of a thixotropic gel followed by a sol state at very high water content.[91] Upon incorporation of high-pressure methane to the wet montmorillonite, X-ray diffraction (XRD) measurements revealed two effects, the formation of methane hydrate crystals and a contraction of the interlayer space from 1.67 nm down to 1.59 nm. A similar contraction of the interlayer space was observed by Guggenheim et al. using the same clay.[92] However, there is a large discrepancy in the literature concerning the location of the methane hydrate crystals. Guggenheim et al. observed the appearance of new XRD peaks at 4º and 8º upon pressurization with methane associated to a new Na-montmorillonite phase with methane hydrate intercalated between 2:1 layers.[92] These observations were confirmed by performing similar experiments with He instead of methane. However, this situation could seem almost impossible considering the values described above from Kim et al., i.e. an interlayer distance of 1.59 nm corresponds to a pore space around 0.6 nm, quite below the lattice parameter of the sI structure in methane hydrate (1.2 nm). Indeed, XRD studies from Kim et al. suggest that methane hydrate formation does not take place in the interlayer space but rather in non-interlamellar voids.[91] However, the presence of a variable stability of the intercalated methane hydrate in the high and low temperature region (via expulsion of methane or water from the interlayer space with a decrease of the *d* space) can explain these discrepancies. The presence of intercalated methane hydrates (IMH) in Smectite clays was also identified by Seo et al. using a wide variety of techniques and confirmed by molecular dynamic simulations.[93–95] MD simulations in expanded montmorillonite structures suggest three different configurations for methane in the interlayer space: i) methane coordinated by H_2O within a quasi-stable methane hydrate cluster, ii) methane coordinated to the siloxane surface of the clay and the H_2O associated with the methane hydrate cluster and iii) methane coordinated by H_2O after diffusing from methane hydrate cluster. It is interesting to note that clay-gas hydrate intercalated have densities similar to those of ocean-floor clay sediments. [92]

As described above for carbon materials and silica, the majority of the studies described in the literature concern methane hydrate formation in pure water. Interestingly, Kumar Saw et al. extended these analyses to bentonite (a clay found in natural geological environments) using synthetic seawater.[71] The incorporation of bentonite clay in the system shortens the induction time of hydrate formation and increases the equilibrium pressure compared to seawater without the clay. The thermodynamic promoting effect of bentonite contrast with the inhibitor effect described before for carbon materials and silica. Compounds which decrease water activity (for instance carbon or silica), by competing for available water molecules act as thermodynamic inhibitors, while compounds that set-up water structures more favorable to hydrate crystal (for instance clays) will act as thermodynamic promoters.[71,93] This unusual behavior allows methane hydrates to be stable, at a given temperature, at pressures below the pure-water hydrate dissociation pressure.

This unusual behavior was also reported for natural and synthetic zeolites (5A and 13X), i.e. hydrate formation is easier in the zeolite solutions.[96] Using different water/zeolites suspension, Kim et al. observed an optimum in the gas consumption for a 0.01 wt.% zeolite 13X solution (4-5 times larger consumption compared to distilled water). Larger water/zeolite ratios gave rise to a decrease in the methane consumption, and indirectly, in the methane hydrate formation due to rapid methane hydrate formation in the interfacial area between the methane gas and the distilled water. To our knowledge this is the only study dealing with methane hydrate formation in the presence of zeolites. However, due to the small size of the inner cavities in these zeolites, these cannot be considered confined hydrates, i.e. hydrate growth must take place preferentially in the interparticle space where gas diffusion and hydrate nucleation are promoted.

4.4. Methane hydrate formation in polymers and metal-organic frameworks

The number of studies dealing with methane hydrate formation in polymers is rather scarce. Wang et al. evaluated the role of surfactants attached to polystyrene nanospheres and observed a promotion in the induction time and in the storage capacity of the formed hydrates after incorporation of the promoter, although in this specific case the polymer was merely a support.[97] Polyurethane was also used in fix bed reactors to improve the water-to-hydrate formation process (up to 54% conversion after 2h), although the process was only studied for CO_2 and no data for methane were reported.[98] The majority of the studies in the literature, although few, deal with coordination polymers, and more specifically with metal-organic frameworks (MOFs). Kim et al. evaluated the methane hydrate formation in metal organic framework MIL-53.[99] Despite the presence of microporosity, methane hydrates could only form in meso- and macropores due to steric restrictions (MIL-53 pores are ≈0.6 nm while sI hydrate lattice is ≈1.2 nm). The presence of methane hydrate formation with sI structure was confirmed by synchrotron high-resolution powder diffraction. Methane hydrates grown in MIL-53 tend to show thermodynamic inhibition, although not that strong as that described in other porous materials such as silica or carbon materials. The exclusion of the methane hydrate formation from the inner micropores and their preferential nucleation in the interparticle space or in the external surface was also described by Casco et al. for a hydrophobic MOF such as ZIF-8.[100] Hydrophilic MOFs (for instance MIL-100) promote water adsorption in the inner cavities, although associated with a strong blocking effect (methane hydrate formation is not promoted in systems where water exhibits a strong interaction with the framework structure). On the contrary, hydrophobic MOFs promote methane hydrate formation, although the hydrate growth takes place in the external surface or in the interparticle space (see **Figure 5**). These systems where water is excluded from the inner cavities (for instance ZIF-8) can be used as a dual system with methane physisorption in the inner empty cavities and methane hydrate formation in the interparticle space, the extend of hydrate formation being tailored by the amount of water incorporated.[100,101]

Methane hydrates formed in MOFs were identified as sI structure using synchrotron X-ray powder diffraction and inelastic neutron scattering.[100] The main difference compared to carbon materials, silica or zeolites as a host structure is the induction period. The presence of large water droplets in the surface of ZIF-8 defines an induction period larger than 2-4 hours depending on the water loading.

In summary, these studies using MOFs, although scarce, clearly anticipate the crucial role not only of the porous structure but also of the surface chemistry defining the water-methane and water-framework interactions, and indirectly, the extent of methane hydrate formation. Taking into account the large diversity of MOFs in terms of porous structure and surface chemistry, these studies open the gate towards the design of a proper MOF material able to achieve an optimum performance for methane storage via hydrate formation (containing large cavities) but with the proper surface chemistry to promote the methane hydrate formation.

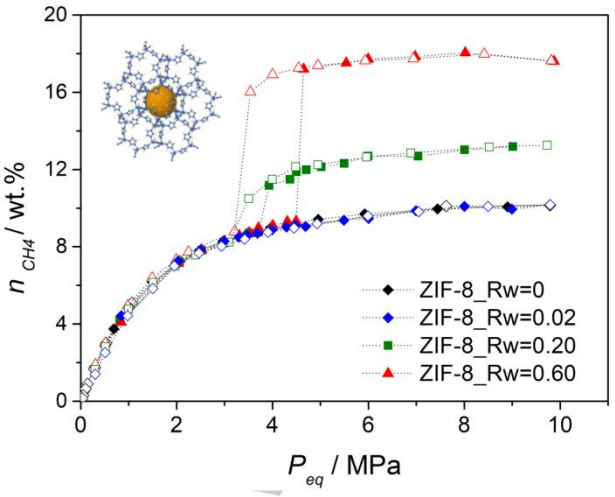

Figure 5. High-pressure methane adsorption isotherms in ZIF-8 after different water loading R_w (g H_2O/g) Reprinted with permission from [100]. Published by The Royal Society of Chemistry.

5. Characterization of methane hydrate in confined spaces

Experimental characterization

The characterization of methane hydrate within the confined environment of nanoporous host structures is more challenging than that of conventional bulk MH for two reasons. Firstly, the size of a nanopore is below 100 nm; which is way below the resolution limit of many visualization techniques. Secondly, the host structure displays an additional phase that could possibly interfere with the measurement signal.

For bulk MH characterization, techniques like *Magnetic Resonance Imaging* (MRI)[102,103] are applicable, that can map ^{1}H non-invasively with a three-dimensional resolution. ^{1}H MRI produces images of hydrogen contained in liquids, but not in methane and solids like ice or MH because of their much shorter transverse relaxation times (T2) which produce a high contrast. In other words, the fact that the material gives observable MRI signals depends on the T2 of the material and the ability of the instrument to capture rapidly decaying signals.[104,105] It allowed an *in situ* monitoring of MH formation from water, for instance showing that the hydrates first form in the center of a pore and then grow along the axis of the vessel.[106] However, only pores in the dimension of several hundred micrometer or larger could be considered. Thus, the resolution is currently only appropriate for bulk systems, and not for nanopores. Similarly, *X-ray computed synchrotron microtomography* can be used to monitor time-resolved MH growth with a 7.5 μm resolution.[107] This method, for instance,

has shown that the hydrate formation starts from dissolved CH_4 rather than from the gas interface. X-ray computed tomography was also used to visualize the decomposition of methane hydrate, its reformations, and the development of flow pathways during dissociation.[108] In general, the spatial resolution of MRI is not high enough to visualize nanopores. Moreover, MRI cannot visualize methane hydrate coexist with ice[103]. On the other hand, X-ray computed tomography (CT) has higher spatial resolution than that of MRI, but it is impossible to distinguish gas hydrate and ice without contrast agents[107] except phase contrast X-ray CT.[109]

To investigate MH formation in nanoporous systems, that means, in a dimension where the confinement effect is relevant, requires techniques working on a molecular level. *High pressure methane adsorption* technique appears to be highly suitable. Although it is not an actual adsorption process, but rather a crystallization phenomenon that is investigated, the characterization is identical to the classical physisorption of porous materials. Basically, defined volumetric amounts of methane gas are dosed in a chamber containing the pre-humidified porous material. Since the experiment is carried out under isothermal condition, any change in the pressure chamber is either due to the adsorption phenomenon or the methane hydrates formation. The isotherm curve is built by recording the volume of gas uptake at each pressure. Increasing pressures define the adsorption branch whereas decreasing pressures define the desorption branch. Using this technique valuable information about the performance of any nanoporous materials can be easily extracted, for instance, the total amount of methane uptake within the porous structure and the experimental stoichiometry of the crystal structure. Moreover, the shape of the isotherm anticipates the dependency of the threshold pressure for methane hydrate formation/dissociation and the pore size, as well as the reversibility of the process. The pressure-time decay curve can also be recorded in order to evaluate the kinetics at each point of the curve. It is important to mention that in order to achieve reliable data a proper selection of the equilibrium parameters is crucial. As described along this review, the methane hydrate formation involves slow kinetics that is reflected in the long time required to complete the full isotherm. The time required for the whole isotherm usually oscillates between 3 up to 30 days (versus 1-2 days for a methane physisorption isotherm), depending on desired resolution of the isotherm (i.e. number of points, final pressure, and so on). [62,63,66]

Inelastic neutron scattering is a tool predominantly sensitive to hydrogen atoms in different sample environments. The spectrum associated to hydrogen atoms from methane physisorbed in a porous material is dominated by its molecular recoil and all the spectroscopic information is washed-out. Nevertheless, the scenery changes when methane molecules are encaged in hydrate crystals. At very low temperature (i.e. 4 K) hydrogen atoms behave like a quantum rotor. The interaction of these hydrogens with the neutron beam causes their rotational transition to excited states, which is reflected in the low energy transfer region of the INS spectrum (see **Figure 6)**. By this technique the methane hydrate footprint can be obtained as long as deuterated water is used for the measurement to avoid any signal overlapping. INS can be used to identify hydrogen atoms in methane either in bulk or confined conditions. Casco et al. have confirmed for the first time the characteristic spectrum of the methane hydrate in metal-organic frameworks and in the cavities of the nanoporous carbon. [62,100]

X-ray powder diffraction has been widely used to identify the crystal structure and the cell parameters of natural, synthetic and confined methane hydrates as well as in their single crystal.[110–114] In principle, single crystal structure analysis is one of the most reliable methods to obtain crystal structure data, however, it has never been applied for the crystals inside confining pores. In the particular case of determining methane hydrate formation by PXRD experiments, a high-pressure experimental setup with a good temperature control is required, usually a high-pressure quartz capillary cell connected to an on-line gas system. Since the X-ray beam has to fully penetrate the capillary, the temperature must be adjusted by a contact-free apparatus, avoiding any ice formation on the external capillary surface. With this technique all crystalline phases and their transformation, e.g. the ice formation and the methane hydrate formation can be evaluated. In principle, the crystal size can be estimated by the Scherrer equation, so that any deviation of MH cell parameters due to confinement effects can be identified. Synchrotron X-ray technique offers the extra advantage of its high intensity that allows shorter collection time (few seconds). For instance, Borchardt et al. observed a reduction of the unit cell parameter of MH when it was formed in mesoporous and microporous carbons.[63] Once formed, the evaluation of the stability of these MH crystals with pressure and temperature can be easily done. Indeed, Casco et.al. have shown the thermal stability of the confined methane hydrate and CO_2 hydrate as well as their molecular exchange capability using in situ SXRD technique.[115]

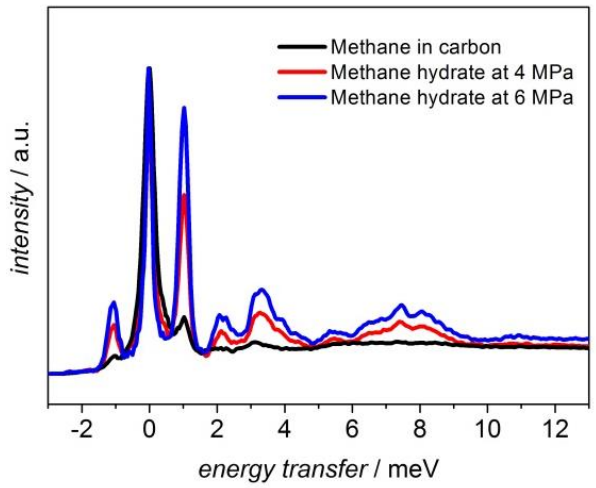

Figure 6. Inelastic Neutron Scattering of methane hydrate. Rotational spectra of hydrogen coming from the methane molecule in wet (deuterated) – activated carbon at different pressures. [62]

Raman spectroscopy is a potent technique to resolve the structure of hydrates, and to obtain information about the composition, i.e. hydration number and the cage occupancy of guest molecules. Based on the fact that methane molecules incorporated in the hydrate lattice are in different chemical environment from that of free gas, the energy of the vibrational modes will differ. For instance, the Raman spectrum for the type I structure exhibits a peak at the frequency 2904 cm^{-1} for methane molecules encaged in the large cavity ($5^{12}6^2$), and a peak at the value of 2915 cm^{-1} for those molecules allocated in the small cavity (5^{12}), whereas methane in vapor phase shows signal at ca. 2918 cm^{-1}.[116] The area of the bands represents the amount of CH_4 in each cavity. In a type I structure there are three times as many large cages as small cages and the occupancy ratio $\theta_{s,CH4}/\theta_{l,CH4}$ is obtained by 3 I_s/I_L (three time the integrated intensity ratio, I_s and I_L are the integrated intensity for small and large cages, respectively), where $\theta_{s,CH4}$ and $\theta_{L,CH4}$ are the absolute fractional occupancies of the small and large cage, respectively. The absolute occupancies cannot be calculated by direct method. However, it can be approximated taking into account the chemical potential of water molecules in the structure I, in the absence of guest-guest interaction and host-lattice distortions[117]. Remember that in sI basic crystal is formed by 46 water molecules containing 8 cavities (2 small and 6 large). When the hydrate is in equilibrium with ice, the following thermodynamics equation can be obtained:[118]

$$\Delta\mu_w(^\circ) = \frac{RT}{46}\left[6\ \ln\left(1-\theta_{l,CH4}\right) + 2\ \ln\left(1-\theta_{s,CH4}\right)\right] \quad \textbf{Eq. 7}$$

$$\Delta\mu_w(^\circ) = \frac{RT}{23}\left[3\ \ln\left(1-\theta_{l,CH4}\right) + \ln\left(1-\theta_{s,CH4}\right)\right] \quad \textbf{Eq. 8}$$

$\Delta\mu_w(^\circ)$ for sI was calculated as 1297 $\pm$ 110 J/mol[119]. Finally, combing **equation 6** and the calculated ratio $\theta_{s,CH4}/\theta_{l,CH4}$, the hydration number (n) for simple hydrate is related to the fractional occupancies of the large and small cavities by **equation 6** [116]:

$$n = \frac{46}{6\theta_{l,CH4}+2\theta_{s,CH4}} = \frac{23}{3\theta_{l,CH4}+\theta_{s,CH4}} \quad \textbf{Eq. 9}$$

Therefore, the ideal hydration number for sI would be 5.75 (46/8). Experimental hydration number was calculated and reported in several works for natural and synthetic sI methane hydrate, either in bulk or confined conditions. The reported values range from about 5.8 to 6.3 when full large cavity occupancy is assumed.[116,120–123]

^{13}C NMR spectrum is very sensitive to identify the environment of methane[124]. It can be analyzed equally to Raman due to the presence of a cage-dependent chemical shift for enclathrated methane[117]. The two signals at −4.2 and −6.7 ppm are typical of methane in the small and large cages, respectively in sI hydrate[123]. The technique provides structural evidence not only for natural methane hydrate but also synthetic methane hydrate in bulk or in confined space. For instance, Chari et al. have recently investigated the composition and phase stability of methane hydrate in bulk, and in solid and hollow silica matrix using RAMAN spectroscopy[125] and ^{13}C NMR spectroscopy to evaluate the replacement of CH_4 by CO_2 in bulk water.[126] Bustin et al. determined by ^{13}C NMR the occupancy of 90% of the small cages in coal moisture, yielding a stoichiometry of ca. $CH_4{\cdot}6H_2O$[123]. The observed broad signal at -4.8 ppm (short T2) could also be assigned to methane dissolved in water, which hints towards weak interaction of these species with the pore wall. At this point it is important to mention that the circumstance that the cavities cannot be completely occupied (the contrary would be a perfect crystal) gives the name “nonstoichiometric hydrates” to clathrate hydrates.[2]

High Pressure Differential Scanning calorimetry (HP-DSC) can be used to investigate the thermodynamic stability of methane hydrate. Usually, it is used for methane hydrate in bulk (in absence of porous materials). Because of the slow kinetics of the formation, the crystals are formed ex-situ and afterwards transferred into the DSC cell under liquid nitrogen[127]. Although the experimental setup required small quantities of sample, the temperature rate must be sufficiently slow to guarantee conditions as close to the equilibrium as possible (e.g. 0.25-1.00 $K{\cdot}min^{-1}$), which leads to long measurement time. The methane hydrate heat of dissociation, ΔH_d, can be calculated at different pressures. Dalmazzonne et al. have used HP-DSC to study the kinetics of formation of natural gas in water-oil-emulsion and in aqueous calcium chloride at pressure 5-11 MPa.[128,129] Although scarcely used, HP-DSC has the potential to evaluate thermodynamic and kinetics parameters in confined crystals, especially in nanoporous carbons since in these systems the interface water/methane is enhanced owing to their extremely high surface area with a complete water to hydrate conversion.

Theoretical calculations and simulations

Bulk methane hydrate structures and dynamics have widely been studied by molecular dynamics (MD) simulations.[130,131] We briefly introduce important findings on bulk simulated water-gas systems in order to understand the results obtained for more complex systems including porous media.

Microsecond simulations on an aqueous phase homogenously saturated with gas have shown that not only the nucleus size, but also the relative position of guest molecules control methane hydrate nucleation.[25] The authors observed an unforeseen molecular order of adsorbed methane molecules in a bowl-like arrangement shortly before hydrate formation. The early formed cages are face-sharing partial small cages favoring the structure II. At a later point, the larger cages appear due to increasing steric constraints and the thermodynamic preference of structure I. It was also calculated that the decomposition rate sensitively depends on the hydration number. Empty cages substantially destabilize the hydrate lattice. Decreasing the occupancy from 95 to 85% increases decomposition rate by 30%.[132] English et al. investigated methane hydrate crystals of a radius of 1.0 – 1.25 nm observing that empty hydrate clusters break up an order of magnitude faster than filled ones.[133] Their simulations also indicated that the methane molecule diffusion from the inner cavities to the crystal surface layer is the rate-controlling step in

hydrate breakup and thus largely affect the methane hydrate dissociation rate. The dissociation process starts with the melting of the large $5^{12}6^2$ cages, followed by the melting of the small 5^{12} cages. The remaining residual hydrate rings are responsible for the so called "memory effect" (i.e. long-lived residual metastable structures).[134]

Simulations on MH in confined spaces, appear to be even more difficult. Sun et al. developed a 3D kinetic simulator for methane hydrate growth and dissociation in porous media (rock grains), taking five components into account; hydrate, gas, aqueous phase, ice and salt.[135] While hydrate formation from gas and aqueous phase occurs in a nearly uniform manner, hydrate formation from gas and ice shows a blocking effect preventing the penetration into the inner region of the core sample. Salt addition leads to disappearance of this blocking phenomenon. When methane hydrate dissociation is simulated it is important to differentiate between the dimensions of a granule, a compressed pellet, a sedimentary rock or MH inside a porous media. In latter, microporous structures behave fundamentally different than meso- and macroporous structures.[136] Heat transfer, the kinetics of phase transformation, gas filtering effects through the porous media, the pore size and the restricted molecular diffusion have to be taken into account. Taking a clay layer and a bulk solution layer as a model, the authors propose that the growth run via i) the migration of dissolved CH_4 to the surface of the clay where semicages are formed, ii) the clathrate grows via stacking fault formation in the region of the bulk solution, and iii) CH_4 diffusion into the nanopores and formation of "interlayer hydrates" and "surface hydrates". This simulation illustrated that hydrate crystals preferably grow at the throats of the pores and that hydroxylated groups of the host material could serve as nucleation spot.[137]

6. Future Potential and Challenges

Natural gas, and its main constituent methane, can be considered as a bridge fuel towards a carbon-free society exhibiting a higher H/C ratio, a higher energy per mass, higher combustion efficiency and a cleaner burning as compared to gasoline. The storage and transportation of methane, however, is restricted by its low density requiring either liquefaction or compression. Methane hydrate displays a nature-inspired alternative for chemical energy storage with a total capacity about 163 m³ of CH_4 within 1 m³ of methane hydrate at STP.

The embedment of MH within porous host structures influences the thermodynamics and the kinetics of MH nucleation, growth and dissociation. It has to be considered that the porous material itself takes up space, thus lowering the gravimetric and volumetric methane storage capacity as compared to the pure solid hydrate. However, the faster kinetics of formation and the higher water to hydrate conversion compared to the bulk water makes methane hydrate in confined space an alternative energy storage system worthy to investigate.[62] Moreover, the storage of methane in wet porous materials can provide higher storage capacities as compared to pure physisorption in dry materials.[62,138] Among the various host structures, carbons, metal-organic frameworks, and silica materials stand out due to their tunable textural properties and surface chemistry, offering a wide range of confined environments to further investigate the MH formation from a fundamental point of view. Although existing in various framework types, zeolites suffer from pore sizes, usually too small to allocate MH inside, likely lowering their applicability as MH host. Clay materials, however, provide a confined environment mimicking that of natural methane hydrate sediments most connaturally.

The following challenges are currently in the focus of researchers all over the world.

Firstly, the identification of an ideal host structure for MH storage. The desired material must aim on high storage capacities, fast formation and dissociation kinetics at discrete and controllable temperature and pressure conditions. The design of the host material needs to consider pore-size, -volume and -connectivity, surface-polarity and –functionalities, as well as materials composition, density and stability.

Secondly, the fundamental understanding of MH growth in confined environments is still in its infancy. Theoretical calculations and simulations on MH nucleation, growth and dissociation within a nanopore are challenging, since the large MH unit cell and the pore environment require huge computational resources. These simulations however, would be of enormous help to understand the unexpected behavior of MH or "methane-hydrate species" in confined spaces. The *in situ* characterization of MH dynamics in confining environments is a current challenge as well. Although the required pressure for MH formation is quite moderate (>30bar) it limits the utilization of many of the standard lab characterization equipment. Furthermore, more experiments and theoretical calculations are necessary to understand the effect of the salt on the confined MH.

Thirdly, the transfer of the knowledge on confined MH to other confined gas hydrate structures such as hydrogen or hydrocarbon hydrates and their evaluation as potential energy storage systems. For instance, storing H_2 in bulk hydrate form is challenging since pure hydrate is stabilized under high pressure (220 MPa at 249K). This inconvenience can be circumvented by the inclusion of THF as a second guest. By this way the stabilization pressure is reduced up to 5 MPa, which is a more reasonable value for a possible application.[2] The effect of confined environments on the nucleation and growth of H_2 hydrate is a field worthy to be explored.

Fourthly, the knowledge gained on confined methane hydrates can be extremely useful in the exploration of new application fields, for instance, the extraction of CH_4 from natural resources (e.g. in sediments) or the coupled CO_2 sequestration using the same hydrate lattice bed in deep sea. This *in-situ* replacement is an ambitious plan that would allow a future of nearly zero carbon emissions.[112] To go further, a more innovative technology may involve the *in-situ* biogenic generation of CH_4 from the entrapped CO_2 to close the cycle.[139] The use of microalgae appears to be promising since they can fix carbon dioxide up to 1.8 times its weight to produce hydrocarbons.[140] Nevertheless, intensive interdisciplinary research is needed to become the idea that, in principle seems to be science fiction, into a palpable reality.

Acknowledgements

LB gratefully acknowledges the Daimler und Benz Stiftung (award number 32-01/16) and the Federal Ministry of Education and Research (Bundesministerium für Bildung und Forschung, BMBF) for support of the Mechanocarb project (award number 03SF0498). MEC acknowledges the Alexander von Humboldt foundation for financial support. J.S.A. acknowledges financial support from MINECO (Project MAT2016-80285-P) and Generalitat Valenciana (PROMETEOII/2014/004).

Keywords: clathrate • gas hydrate • porous • natural gas • energy storage

[1] H. Davy, *Philos. Trans. R. Soc. London* **1811**, *101*, 155–162.
[2] E. Dendy Sloan, C. A. Koh, E. D. Sloan, C. A. Koh, E. Dendy Sloan, C. A. Koh, *Clathrate Hydrates of Natural Gases*, **2007**.
[3] E. G. Hammerschmidt, *Ind. Eng. Chem.* **1934**, *26*, 851–855.
[4] Y. Makogon, *No Hydrates of Natural Gas*, PennWell, Tulsa, Oklahoma, **1981**.
[5] J. B. Klauda, S. I. Sandler, *Energy & Fuels* **2005**, *19*, 459–470.
[6] E. D. Sloan, *Nature* **2003**, *426*, 353–363.
[7] Y. Konno, T. Fujii, A. Sato, K. Akamine, M. Naiki, Y. Masuda, K. Yamamoto, J. Nagao, *Energy and Fuels* **2017**, *31*, 2607–2616.
[8] Y. Zhang, X. Li, Y. Wang, Z. Chen, G. Li, *Energies* **2017**, *10*, DOI 10.3390/en10040561.
[9] T. Collett, J.-J. Bahk, R. Baker, R. Boswell, D. Divins, M. Frye, D. Goldberg, J. Husebø, C. Koh, M. Malone, et al., *J. Chem. Eng. Data* **2015**, *60*, 319–329.
[10] J. Javanmardi, M. Moshfeghian, *Appl. Therm. Eng.* **2003**, *23*, 845–857.
[11] A. Eslamimanesh, A. H. Mohammadi, D. Richon, P. Naidoo, D. Ramjugernath, *J. Chem. Thermodyn.* **2012**, *46*, 62–71.
[12] N. Goel, *J. Pet. Sci. Eng.* **2006**, *51*, 169–184.
[13] I. Chatti, A. Delahaye, L. Fournaison, J.-P. Petitet, *Energy Convers. Manag.* **2005**, *46*, 1333–1343.
[14] P. Englezos, J. D. Lee, *Korean J. Chem. Eng.* **2005**, *22*, 671–681.
[15] H. Mimachi, M. Takahashi, S. Takeya, Y. Gotoh, A. Yoneyama, K. Hyodo, T. Takeda, T. Murayama, *Energy & Fuels* **2015**, *29*, 4827–4834.
[16] "NGH | Close-up Technology | MES Technology | MES," can be found under https://www.mes.co.jp/english/mes_technology/ngh.html, **n.d.**
[17] G. Rehder, R. Eckl, M. Elfgen, A. Falenty, R. Hamann, N. Kähler, W. F. Kuhs, H. Osterkamp, C. Windmeier, *Energies* **2012**, *5*, 2499–2523.
[18] A. Celzard, J. F. Marêché, *Fuel* **2006**, *85*, 957–966.
[19] J. H. Van der Waals, J. C. Platteeuw, *Adv. Chem. Physics, Vol. 2* **2007**, 1–57.
[20] P. Henry, M. Thomas, M. Ben Clennell, *J. Geophys. Res.* **1999**, *104*, 23005.
[21] M. A. Clarke, M. Pooladi-Darvish, P. R. Bishnoi, *Ind. Eng. Chem. Res.* **1999**, *38*, 2485–2490.
[22] D. Kim, H. Lee, *Korean J. Chem. Eng.* **2016**, *33*, 1977–1988.
[23] T. A. Strobel, K. C. Hester, C. A. Koh, A. K. Sum, E. D. Sloan, *Chem. Phys. Lett.* **2009**, *478*, 97–109.
[24] A. Vysniauskas, P. R. Bishnoi, *Chem. Eng. Sci.* **1983**, *38*, 1061–1072.
[25] M. R. Walsh, C. A. Koh, E. D. Sloan, A. K. Sum, D. T. Wu, *Science (80-.).* **2009**, *326*, 1095–1098.
[26] N.-J. Kim, J. Hwan Lee, Y. S. Cho, W. Chun, *Energy* **2010**, *35*, 2717–2722.
[27] Y. Zhong, R. E. Rogers, *Chem. Eng. Sci.* **2000**, *55*, 4175–4187.
[28] R. Rogers, G. Zhang, J. Dearman, C. Woods, *J. Pet. Sci. Eng.* **2007**, *56*, 82–88.
[29] K. Okutani, Y. Kuwabara, Y. H. Mori, *Chem. Eng. Sci.* **2008**, *63*, 183–194.
[30] J. S. Zhang, S. Lee, J. W. Lee, *J. Colloid Interface Sci.* **2007**, *315*, 313–318.
[31] K. Watanabe, S. Imai, Y. H. Mori, *Chem. Eng. Sci.* **2005**, *60*, 4846–4857.
[32] P. Gayet, C. Dicharry, G. Marion, A. Graciaa, J. Lachaise, A. Nesterov, *Chem. Eng. Sci.* **2005**, *60*, 5751–5758.
[33] P. Di Profio, S. Arca, R. Germani, G. Savelli, *Chem. Eng. Sci.* **2005**, *60*, 4141–4145.
[34] W. Wang, C. L. Bray, D. J. Adams, A. I. Cooper, *J. Am. Chem. Soc.* **2008**, *130*, 11608–11609.
[35] H. P. Veluswamy, A. Kumar, R. Kumar, P. Linga, *Appl. Energy* **2017**, *188*, 190–199.
[36] H. P. Veluswamy, Q. W. Hong, P. Linga, *Cryst. Growth Des.* **2016**, *16*, 5932–5945.
[37] P. R. Bishnoi, P. D. Dholabhai, *Fluid Phase Equilib.* **1999**, *158*, 821–827.
[38] X. Lang, S. Fan, Y. Wang, *J. Nat. Gas Chem.* **2010**, *19*, 203–209.
[39] P. D. Menten, W. R. Parrish, E. D. Sloan, *Ind. Eng. Chem. Process Des. Dev.* **1981**, *20*, 399–401.
[40] J. P. Lederhos, J. P. Long, A. Sum, R. L. Christiansen, E. D. Sloan, *Chem. Eng. Sci.* **1996**, *51*, 1221–1229.
[41] C. Xiao, H. Adidharma, *Chem. Eng. Sci.* **2009**, *64*, 1522–1527.
[42] J.-H. Sa, G.-H. Kwak, K. Han, D. Ahn, S. J. Cho, J. D. Lee, K.-H. Lee, *Sci. Rep.* **2016**, *6*, 31582.
[43] J. Kim, H. Kim, Y. hoon Sohn, D. Chang, Y. Seo, S.-P. Kang, *J. Pet. Sci. Eng.* **2017**, *154*, 114–125.
[44] M. Alcoutlabi, G. B. McKenna, *J. Phys. Condens. Matter* **2005**, *17*, R461–R524.
[45] G. Sastre, A. Corma, *J. Mol. Catal. A Chem.* **2009**, *305*, 3–7.
[46] E. DEROUANE, *J. Catal.* **1988**, *110*, 58–73.
[47] C. Zicovich-Wilson, J. H. Planelles, W. Jaskóalski, *Int. J. Quantum Chem.* **1994**, *50*, 429–444.
[48] C. Alba-Simionesco, B. Coasne, G. Dosseh, G. Dudziak, K. E. Gubbins, R. Radhakrishnan, M. Sliwinska-Bartkowiak, *J. Phys. Condens. Matter* **2006**, *18*, R15–R68.
[49] G. H. Findenegg, S. Jähnert, D. Akcakayiran, A. Schreiber, *ChemPhysChem* **2008**, *9*, 2651–2659.
[50] C. K. Das, J. K. Singh, *J. Chem. Phys.* **2014**, *140*, 204703.
[51] C. K. Das, J. K. Singh, *Theor. Chem. Acc.* **2013**, *132*, 1351.
[52] Y. Long, J. C. Palmer, B. Coasne, M. Śliwinska-Bartkowiak, K. E. Gubbins, *Phys. Chem. Chem. Phys.* **2011**, *13*, 17163.

[53] P. Linga, N. Daraboina, J. A. Ripmeester, P. Englezos, *Chem. Eng. Sci.* **2012**, *68*, 617–623.
[54] O. Fandiño, L. Ruffine, *Fuel* **2014**, *117*, 442–449.
[55] R. Andersen, M. Llamedo, B. Tohidi, R. W. Burgass, *J. Phys. Chem. B* **2003**, *107*, 3500–3506.
[56] K. V. Kumar, K. Preuss, M.-M. Titirici, F. Rodríguez-Reinoso, *Chem. Rev.* **2017**, *117*, 1796–1825.
[57] M. E. Casco, M. Martínez-Escandell, E. Gadea-Ramos, K. Kaneko, J. Silvestre-Albero, F. Rodríguez-Reinoso, M. Mart, E. Gadea-Ramos, K. Kaneko, J. Silvestre-Albero, et al., *Chem. Mater.* **2015**, *27*, 959–964.
[58] H. M. F. Rodriguez-Reinosso, *Activated Carbon*, Elsevier, Boston, **2006**.
[59] J. Miyawaki, T. Kanda, T. Suzuki, T. Okui, Y. Maeda, K. Kaneko, *J. Phys. Chem. B* **1998**, *102*, 2187–2192.
[60] L. Zhou, Y. Sun, Y. Zhou, *AIChE J.* **2002**, *48*, 2412–2416.
[61] A. Perrin, A. Celzard, J. F. Marêché, G. Furdin, *Energy and Fuels* **2003**, *17*, 1283–1291.
[62] M. E. Casco, J. Silvestre-Albero, A. J. Ramírez-Cuesta, F. Rey, J. L. Jordá, A. Bansode, A. Urakawa, I. Peral, M. Martínez-Escandell, K. Kaneko, et al., *Nat. Commun.* **2015**, *6*, 6432.
[63] L. Borchardt, W. Nickel, M. E. Casco, I. Senkovska, V. Bon, D. Wallacher, N. Grimm, S. Krause, J. J. J. Silvestre-Albero, D. Wallacher, et al., *Phys. Chem. Chem. Phys.* **2016**, *18*, 20607–20614.
[64] A. Siangsai, P. Rangsunvigit, B. Kitiyanan, S. Kulprathipanja, P. Linga, *Chem. Eng. Sci.* **2015**, *126*, 383–389.
[65] M. J. D. M. J. D. Mahboub, A. Ahmadpour, H. Rashidi, *Ranliao Huaxue Xuebao/Journal Fuel Chem. Technol.* **2012**, *40*, 385–389.
[66] M. E. Casco, C. Cuadrado-Collados, M. Martínez-Escandell, F. Rodríguez-Reinoso, J. Silvestre-Albero, *Carbon N. Y.* **2017**, *123*, 299–301.
[67] V. Govindaraj, D. Mech, G. Pandey, R. Nagarajan, J. S. Sangwai, *J. Nat. Gas Sci. Eng.* **2015**, *26*, 810–818.
[68] L. Yan, G. Chen, W. Pang, J. Liu, *J. Phys. Chem. B* **2005**, *109*, 6025–6030.
[69] H. Ganji, M. Manteghian, M. R. Omidkhah, H. R. Mofrad, *Fuel* **2007**, *86*, 434–441.
[70] J. Li, D. Liang, K. Guo, R. Wang, S. Fan, *Energy Convers. Manag.* **2006**, *47*, 201–210.
[71] S. B. Cha, H. Ouar, T. R. Wildeman, E. D. Sloan, *J. Phys. Chem.* **1988**, *92*, 6492–6494.
[72] E. A. Smelik, H. E. King, *Am. Mineral.* **1997**, *82*, 88–98.
[73] P. Babu, D. Yee, P. Linga, A. Palmer, B. C. Khoo, T. S. Tan, P. Rangsunvigit, *Energy & Fuels* **2013**, *27*, 3364–3372.
[74] J.-W. Jung, J. C. Santamarina, *J. Cryst. Growth* **2012**, *345*, 61–68.
[75] S.-S. Park, S.-B. Lee, N.-J. Kim, *J. Ind. Eng. Chem.* **2010**, *16*, 551–555.
[76] S. Lim, S. B. Riffat, S. Park, S. Oh, W. Chun, N. Kim, *Int. J. Energy Res.* **2014**, *38*, 374–379.
[77] Y. P. Handa, D. Y. Stupin, *J. Phys. Chem.* **1992**, *96*, 8599–8603.
[78] C. Cuadrado-Collados, F. Fauth, I. Such-Basañez, M. Martínez-Escandell, J. Silvestre-Albero, *Microporous Mesoporous Mater.* **2017**.
[79] Y. Seo, H. Lee, T. Uchida, *Langmuir* **2002**, *18*, 9164–9170.
[80] T. Uchida, T. Ebinuma, T. Ishizaki, *J. Phys. Chem. B* **1999**, *103*, 3659–3662.
[81] T. Uchida, T. Ebinuma, S. Takeya, J. Nagao, H. Narita, *J. Phys. Chem. B* **2002**, *106*, 820–826.
[82] Y. P. Handa, *J. Chem. Thermodyn.* **1986**, *18*, 891–902.
[83] G. Hu, Y. Ye, C. Liu, Q. Meng, J. Zhang, S. Diao, *Fuel Process. Technol.* **2011**, *92*, 1617–1622.
[84] V. P. Mel'nikov, L. S. Podenko, A. N. Nesterov, A. O. Drachuk, N. S. Molokitina, A. M. Reshetnikov, *Dokl. Chem.* **2016**, *466*, 53–56.
[85] A. Hachikubo, S. Takeya, E. Chuvilin, V. Istomin, *Phys. Chem. Chem. Phys.* **2011**, *13*, 17449.
[86] P. Linga, C. Haligva, S. C. Nam, J. A. Ripmeester, P. Englezos, *Energy & Fuels* **2009**, *23*, 5496–5507.
[87] V. C. Nair, S. Ramesh, G. A. Ramadass, J. S. Sangwai, *J. Pet. Sci. Eng.* **2016**, *147*, 547–559.
[88] Y. Jin, Y. Konno, J. Nagao, *Energy and Fuels* **2012**, *26*, 2242–2247.
[89] P. S. R. Prasad, *J. Chem. Eng. Data* **2014**, *60*, 304–310.
[90] P. S. R. Prasad, Y. Sowjanya, V. Dhanunjana Chari, *J. Phys. Chem. C* **2014**, *118*, 7759–7764.
[91] D. Kim, Y.-H. Ahn, S.-J. Kim, J. Y. Lee, J. Lee, Y. Seo, H. Lee, *J. Phys. Chem. C* **2015**, *119*, 22148–22153.
[92] S. Guggenheim, A. F. K. van Groos, *Geology* **2003**, *31*, 653–656.
[93] Y. Seo, J. Seol, S.-H. Yeon, D.-Y. Koh, M. Cha, S.-P. Kang, Y.-T. Seo, J. Bahk, J. Lee, H. Lee, *J. Chem. Eng. Data* **2009**, *54*, 1284–1291.
[94] R. T. Cygan, S. Guggenheim, A. F. Koster van Groos, *J. Phys. Chem. B* **2004**, *108*, 15141–15149.
[95] Q. Zhou, X. Lu, X. Liu, L. Zhang, H. He, J. Zhu, P. Yuan, *J. Colloid Interface Sci.* **2011**, *355*, 237–242.
[96] N. Kim, S. Park, S. Shin, J. Hyun, W. Chun, *Int. J. Energy Res.* **2015**, *39*, 26–32.
[97] F. Wang, G.-Q. Liu, H.-L. Meng, G. Guo, S.-J. Luo, R.-B. Guo, *ACS Sustain. Chem. Eng.* **2016**, *4*, 2107–2113.
[98] P. Babu, R. Kumar, P. Linga, *Environ. Sci. Technol.* **2013**, *47*, 13191–13198.
[99] D. Kim, Y.-H. Ahn, H. Lee, *J. Chem. Eng. Data* **2015**, *60*, 2178–2185.
[100] M. E. Casco, F. Rey, J. L. Jordá, S. Rudić, F. Fauth, M. Martínez-Escandell, F. Rodríguez-Reinoso, E. V. Ramos-Fernández, J. Silvestre-Albero, S. Rudic, et al., *Chem. Sci.* **2016**, *7*, 3658.
[101] L. Mu, B. Liu, H. Liu, Y. Yang, C. Sun, G. Chen, *J. Mater. Chem.* **2012**, *22*, 12246–12252.
[102] S. Wang, M. Yang, P. Wang, Y. Zhao, Y. Song, *Energy & Fuels* **2015**, *29*, 3251–3256.
[103] I. L. Moudrakovski, J. A. Ripmeester, in *eMagRes*, John Wiley & Sons, Ltd, Chichester, UK, **1996**, pp. 1–10.
[104] J. Zhao, Q. Lv, Y. Li, M. Yang, W. Liu, L. Yao, S. Wang, Y. Zhang, Y. Song, *Magn. Reson. Imaging* **2015**, *33*, 485–490.
[105] M. Yang, Y. Song, Y. Zhao, Y. Liu, L. Jiang, Q. Li, *Magn. Reson. Imaging* **2011**, *29*, 1007–1013.
[106] Y. Song, S. Wang, M. Yang, W. Liu, J. Zhao, S. Wang, *Fuel* **2015**, *140*, 126–135.
[107] P. B. Kerkar, K. Horvat, K. W. Jones, D. Mahajan, *Geochemistry,*

Geophys. Geosystems **2014**, *15*, 4759–4768.
[108] A. Gupta, G. J. Moridis, T. J. Kneafsey, E. D. Sloan, *Energy & Fuels* **2009**, *23*, 5958–5965.
[109] S. Takeya, A. Yoneyama, K. Ueda, K. Hyodo, T. Takeda, H. Mimachi, M. Takahashi, T. Iwasaki, K. Sano, H. Yamawaki, *J. Phys. Chem. C* **2011**, *115*, 16193–16199.
[110] R. K. McMullan, G. A. Jeffrey, *J. Chem. Phys.* **1965**, *42*, 2725–2732.
[111] J. Shu, X. Chen, I. M. Chou, W. Yang, J. Hu, R. J. Hemley, H. K. Mao, *Geosci. Front.* **2011**, *2*, 93–100.
[112] M. T. Kirchner, R. Boese, W. E. Billups, L. R. Norman, *J. Am. Chem. Soc.* **2004**, *126*, 9407–9412.
[113] S.-H. Yeon, J. Seol, Y. Seo, Y. Park, D.-Y. Koh, K.-P. Park, D.-G. Huh, J. Lee, H. Lee, *J. Phys. Chem. B* **2009**, *113*, 1245–1248.
[114] S. Takeya, H. Fujihisa, Y. Gotoh, V. Istomin, E. Chuvilin, H. Sakagami, A. Hachikubo, *J. Phys. Chem. C* **2013**, *117*, 7081–7085.
[115] M. E. Casco, J. L. Jordá, F. Rey, F. Fauth, M. Martinez-Escandell, F. Rodríguez-Reinoso, E. V. Ramos-Fernández, J. Silvestre-Albero, *Chem. - A Eur. J.* **2016**, *22*, 10028–10035.
[116] A. K. Sum, R. C. Burruss, E. D. Sloan, *J. Phys. Chem. B* **1997**, *101*, 7371–7377.
[117] J. A. Ripmeester, C. I. Ratcliffe, *J. Phys. Chem.* **1988**, *92*, 337–339.
[118] J. H. Van der Waals, J. C. Platteeuw, *Nature* **1959**, *183*, 462.
[119] D. W. Davidson, Y. P. Handa, J. A. Ripmeester, *J. Phys. Chem.* **1986**, *90*, 6549–6552.
[120] M. Kida, A. Hachikubo, H. Sakagami, H. Minami, A. Krylov, S. Yamashita, N. Takahashi, H. Shoji, O. Khlystov, J. Poort, et al., *Geochemistry, Geophys. Geosystems* **2009**, *10*, n/a-n/a.
[121] S. Circone, S. H. Kirby, L. A. Stern, *J. Phys. Chem. B* **2005**, *109*, 9468–9475.
[122] K. C. Hester, R. M. Dunk, S. N. White, P. G. Brewer, E. T. Peltzer, E. D. Sloan, *Geochim. Cosmochim. Acta* **2007**, *71*, 2947–2959.
[123] A. M. M. Bustin, R. M. Bustin, I. L. Moudrakovskim, S. Takeya, J. A. Ripmeester, *Energy and Fuels* **2016**, *30*, 88–97.
[124] A. Kleinhammes, S.-H. Mao, X.-J. Yang, X.-P. Tang, H. Shimoda, J. P. Lu, O. Zhou, Y. Wu, *Phys. Rev. B* **2003**, *68*, 75418.
[125] V. D. Chari, P. S. R. Prasad, S. R. Murthy, *Spectrochim. Acta Part A Mol. Biomol. Spectrosc.* **2014**, *120*, 636–641.
[126] S. Lee, S. Park, Y. Lee, Y. Seo, *Chem. Eng. J.* **2013**, *225*, 636–640.
[127] A. Gupta, J. Lachance, E. D. Sloan, C. A. Koh, *Chem. Eng. Sci.* **2008**, *63*, 5848–5853.
[128] D. Dalmazzone, N. Hamed, C. Dalmazzone, *Chem. Eng. Sci.* **2009**, *64*, 2020–2026.
[129] M. Kharrat, D. Dalmazzone, *J. Chem. Thermodyn.* **2003**, *35*, 1489–1505.
[130] J. O. Titiloye, N. T. Skipper, *Chem. Phys. Lett.* **2000**, *329*, 23–28.
[131] S.-H. Park, G. Sposito, *J. Phys. Chem. B* **2003**, *107*, 2281–2290.
[132] E. M. Myshakin, H. Jiang, R. P. Warzinski, K. D. Jordan, *J. Phys. Chem. A* **2009**, *113*, 1913–1921.
[133] N. J. English, J. K. Johnson, C. E. Taylor, *J. Chem. Phys.* **2005**, *123*, 244503.
[134] D. Bai, X. Zhang, G. Chen, W. Wang, *Energy Environ. Sci.* **2012**, *5*, 7033.
[135] X. Sun, K. K. Mohanty, *Chem. Eng. Sci.* **2006**, *61*, 3476–3495.
[136] S. Y. Misyura, *Sci. Rep.* **2016**, *6*, 30324.
[137] K.-F. Yan, X.-S. Li, Z.-Y. Chen, Z.-M. Xia, C.-G. Xu, Z. Zhang, *Langmuir* **2016**, *32*, 7975–7984.
[138] M. L. Zanota, L. Perier-Camby, F. Chauvy, Y. Brullé, J. M. Herri, *ICGH 5* **2005**, 2–6.
[139] V. Honkalas, A. Dabir, P. K. Dhakephalkar, Springer, Cham, **2015**, pp. 235–262.
[140] K. Gao, K. R. McKinley, *J. Appl. Phycol.* **1994**, *6*, 45–60.